Characterization and reduction of audible magnetic noise due to PWM supply in induction machines

J. Le Besnerais, V. Lanfranchi, M. Hecquet, and P. Brochet, *Member, IEEE*

***Abstract*— This paper derives the analytical characterization of Maxwell radial vibrations due to Pulse-Width Modulation (PWM) supply in induction machines, and especially in traction motors supplied with an asynchronous switching frequency. The number of nodes and the velocity of these particular force waves are experimentally validated by visualizing some operational deflection shapes of the stator. It is shown that according to the switching frequency, these forces can be responsible for high magnetic noise levels during starting and braking. A simple rule to avoid PWM noise is then proposed, and applied to an industrial traction motor.**

Experimental results show that the choice of the switching frequency can have a 15 dB impact on the sound power level emitted by the motor during starting, and that a lower switching frequency can sometimes lead to lower magnetic noise. In agreement with analytical predictions, the new proposed switching frequency that avoids resonances between PWM exciting forces and corresponding stator modes reduces magnetic noise of 5 dB during starting.

***Index Terms*— Induction machine, Pulse-Width Modulation, magnetic noise, vibrations, Maxwell forces.**

NOMENCLATURE

f_c	PWM switching frequency
f_m	m-th stator circumferential mode natural frequency
f_s	Stator current fundamental frequency
f_n^s	Stator current n-th time harmonic
f_{mm}^s	Stator magnetomotive force (mmf)
F_0	Stator fundamental mmf
F_n	Stator mmf due to PWM harmonic
i_q^s	q-th stator phase current
p	Number of pole pairs
q_s	Number of stator phases
s	Fundamental slip
α_s	Angular position in stator steady frame
Λ	Air-gap permeance per unit area
μ_0	Air-gap magnetic permeability

I. INTRODUCTION

Manuscript received March 21, 2009. Accepted for publication June 22, 2009. Copyright ©2009 IEEE. Personal use of this material is permitted. However, permission to use this material for any other purposes must be obtained from the IEEE by sending a request to pubs-permissions@ieee.org. This work was supported in part by the French Agence De l'Environnement et de la Maîtrise de l'Energie.

J. Le Besnerais is with the Laboratoire d'Electrotechnique et d'Electronique de Puissance (L2EP), Ecole Centrale de Lille, FRANCE (e-mail:jean.le_besnerais@centraliens.net, website:http://l2ep.univ-lille1.fr/pagesperso/lebesnerais/).

V. Lanfranchi is with the Laboratoire d'Electromécanique de Compiègne (LEC), UTC, Compiègne, FRANCE (e-mail: vincent.lanfranchi@utc.fr).

M. Hecquet and P. Brochet are also with the L2EP (e-mail: michel.hecquet@ec-lille.fr and pascal.brochet@ec-lille.fr).

Acoustic comfort is an important factor when designing an electrical transport system: passengers tend to be placed closer to the engine to increase the vehicle capacity, and urban vehicle often drive close from frontage residents and passers-by. As progress is being made in mechanical and aerodynamic noise reduction, the full understanding of magnetic noise generation becomes crucial. This particular source of noise, whose tonalities are penalized by IEC 60034-9 norm, is mainly due to the air-gap radial Maxwell forces that excite the stator in the audible range.

The spectrum composition of these exciting magnetic forces comes from several harmonic sources:

1) the magnetomotive force (mmf) force harmonics due to the discretization of stator and rotor winding in slots, whose influence can be minimized for instance by a proper short-pitch of the stator winding
2) the air-gap permeance harmonics due to slotting effects, whose influence on acoustic noise depend on the slot numbers [1] and slot opening widths [2]
3) the air-gap permeance harmonics due to saturation effects, whose influence can also be minimized by a proper choice of the slot combination and a reduction of saturation level [3]
4) the air-gap permeance harmonics due to dynamic and eccentricity effects
5) the stator mmf harmonics due to Pulse-Width Modulation (PWM) harmonics in stator currents in variable-speed applications, and especially traction motors

This paper focuses on the latter source. Indeed, the exciting force harmonics of type 1) to 4) have all frequencies that are proportional to the stator supply frequency f_s, so at starting they have very low frequencies out of the human ear sensitivity range (dBA weighting). On the contrary, the exciting frequencies of type 5) are not null at starting as PWM strategies always start with an asynchronous phase. Furthermore, mechanical and aerodynamic noise sources are also negligible when $f_s \approx 0$, so the main source of acoustic noise at starting of any electrical motor is due to PWM.

In [4], the analytical characteristics of PWM magnetic forces are not extensively given, as resonances with the $2p$ stator circumferential mode are not considered, and they are not experimentally validated. Furthermore, the most dangerous force waves are not clearly identified, and no rule is given to avoid resonances between PWM magnetic force waves and mechanical structure.

This paper presents the exhaustive analytical characterization of Maxwell vibrations due to PWM, on the ground of a fully analytical vibro-acoustic model of the induction

machine. Their characteristics (velocity, number of nodes) are experimentally validated by visualizing the stator stack deflections at some given frequencies.

On the ground of these analytical results, a simple rule in order to avoid strong resonances due to PWM is then proposed, and applied to a 250 kW traction motor. Some experiments are finally run to measure the sound power level radiated by the motor during starting using several different switching frequencies. It is shown that in agreement with the proposed analytical law, changing the switching frequency from 1280 Hz to 1000 Hz significantly reduces the noise level on test motor. Moreover, a 15 dB variation can be observed according to the value of the switching frequency.

II. Characterization of magnetic noise due to PWM

A. Expression of radial Maxwell forces

Neglecting tangential component of the Maxwell tensor and magnetostrictive effect, the radial exciting pressure P_M which is supposed to be the only magnetic noise source can be approximated by [5], [6], [7]

$$P_M = B_g^2/(2\mu_0) \tag{1}$$

where B_g is the radial air-gap flux density. Assuming that the rotor is not skewed, and neglecting end-effects, this force is independent of the axial direction and can therefore only excite some circumferential modes of the stator stack, which can be modeled by an equivalent ring as a first approximation [6], [8]. Developing the magnetic pressure (1) in two-dimensional Fourier series, it can be expressed as a sum of progressive force waves of frequency f and space frequency m (spatial order) :

$$P_M(t,\alpha_s) = \sum_{m,f} A_{mf}\cos(2\pi f t - m\alpha_s + \phi_{mf}) \tag{2}$$

A magnetic noise resonance occurs at two conditions [9]: the order m of the force harmonic must be the same as the circumferential mode number of the stator (e.g. $m = 2$ for the elliptical mode), and the frequency of the force harmonic must be the same as the frequency of the natural frequency of the stator mode under consideration. There exists an infinite number of force harmonics, but the magnitude of the vibration waves that they generate are inversely proportional to m^4 [7], so that only the lowest spatial orders forces lead to significant vibration and noise (0 to 4 for traction motors).

In order to predict magnetic noise resonances, one must therefore analytically calculate the Fourier development of P_M. This requires an analytical model of the air-gap radial flux density distribution, for instance a permeance / magnetomotive force (mmf) decomposition [10]. In no-load case, this decomposition can be written as [11]

$$B_g(t,\alpha_s) = \Lambda(t,\alpha_s) f^s_{mm}(t,\alpha_s) = \Lambda(t,\alpha_s)\sum_{q=1}^{q_s} i^s_q(t) N^s_q(\alpha_s) \tag{3}$$

where Λ is the air-gap permeance per unit area, f^s_{mm} is the stator mmf, and N^s_q is the 2-D turns function or winding distribution function associated to the stator q-th phase flowed with current i^s_q.

B. PWM force waves

In this section, the magnitude, the frequency and the spatial order of main magnetic forces due to PWM are going to be determined analytically.

Schematically, in the general case, any Maxwell pressure harmonic P_h can be written from (1) and (3) in no-load sinusoidal case as

$$P_h = \Lambda_h \Lambda_{h'} F_h F_{h'}/(2\mu_0) \tag{4}$$

where Λ_h and $\Lambda_{h'}$ are permeance fundamental (Λ_0) or harmonics which can come either from stator slotting (Λ_s), rotor slotting (Λ_r) or their interaction (Λ_{sr}), F_h and $F_{h'}$ are stator mmf fundamental (F_0) or harmonics (F_n) which either come from the discretized distribution of stator winding in slots (space harmonics) or from the PWM stator current harmonics (time harmonics).

Neglecting the slotting effects which are responsible for slotting harmonics ($\Lambda(t,\alpha_s) = \Lambda_0$), a phenomenon whose characterization and reduction has been treated in [4], [2], and assuming that the stator winding is ideal (no winding harmonics), one can easily find the main Maxwell pressure harmonics that are due to PWM. These particular force waves are called pure PWM force waves, contrary to slotting PWM waves which come from the combination of slotting permeance harmonics and PWM stator mmf harmonics due to PWM current harmonics [12].

The magnitude of these pure PWM force waves are therefore given by

$$P_{nn'} = \Lambda_0^2 F_n F_{n'}/(2\mu_0) \tag{5}$$

where F_n and $F_{n'}$ are two stator mmf waves coming from fundamental current or its PWM harmonics. Of course, these force waves are the greater when one of the lines F_n or $F_{n'}$ is the fundamental stator mmf F_0. The largest pure PWM forces magnitude are therefore given by

$$P_{0n} = \Lambda_0^2 F_0 F_n/(2\mu_0) \tag{6}$$

To predict resonance effects, characterizing the PWM force waves magnitude is not sufficient as one must know both their frequency and spatial order. These can be determined by combining the fundamental flux density of spatial order p and frequency f_s with a flux density harmonic due to a PWM current harmonics, of spatial order p and frequency f^s_n. The resulting waves are given by the cosine product formula, and their properties are summarized in Table I. In that table, the symbol η_s takes the value ± 1, indicating the propagation direction of the harmonic flux density due to PWM stator current harmonic of frequency f^s_n. For each current harmonic, two groups of force harmonics are obtained, namely F^-_{pwm} and F^+_{pwm}, which have the same magnitude P_{0n}.

TABLE I

LARGEST PURE PWM FORCE LINES EXPRESSION.

Name	Frequency f	Spatial order m
F^{-}_{pwm}	$f_s - \eta_s f^s_n$	$p - p = 0$
F^{+}_{pwm}	$f_s + \eta_s f^s_n$	$p + p = 2p$

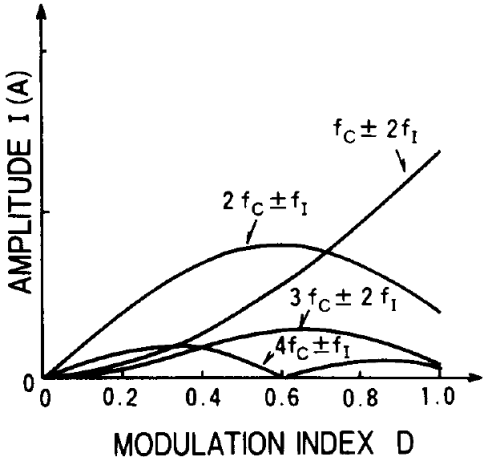

Fig. 1. Evolution of regular sampling PWM current harmonics magnitude in function of the modulation index, f_I being the supply frequency (graph from [13]).

All pure PWM force harmonics have therefore either a spatial order of 0 or $2p$ [4]. They can only resonate with the stator breathing mode $m = 0$, or the stator circumferential mode $m = 2p$ (for traction motors $p = 2$ or $p = 3$ which gives the mode number 4 or 6). Note that in Table I, the frequencies of the force waves can be negative: the frequency sign gives the propagation direction of the wave.

In the case of an intersective PWM with triangular carrier, the harmonics f^s_n can be written as [13]:

$$f^s_n = n_1 f_s \pm n_2 f_c \quad \text{where } n_1 \text{ and } n_2 \text{ have an opposite parity} \tag{7}$$

where f_c is the chopping frequency. The current harmonics of highest magnitude depend on the carrier type, and on the modulation index. As an example, the main group of current harmonics at low modulation index is $f_c \pm f_s$ and $f_c \pm 2f_s$ for a forward saw-tooth carrier shape, while it is $2f_c \pm f_s$ for a standard symmetrical triangular carrier. Furthermore, the magnitude of current harmonics and of the associated mmf harmonics F_n also vary with the modulation index: for a regular sampling intersective PWM, the group $2f_c \pm f_s$ dominates in starting phase, whereas at maximum speed, it is the group $f_c \pm 2f_s$ (see Fig. 1).

PWM magnetic noise is the most annoying at low speed when the aerodynamic noise is lower. In the asynchronous case with a triangular carrier, the noisiest PWM lines can therefore be characterized by Table II.

The expressions of these lines are obtained by replacing $\eta_s f^s_n$ of Table I by the corresponding current harmonics. One must be aware of the propagation direction of the mmf waves $\eta_s = \pm 1$: in the same way that the propagation direction of a space harmonic mmf depends on the space harmonic number, the traveling direction of a time harmonic mmf depends on the frequency (see Fig. 2).

TABLE II

HIGHEST PURE PWM FORCE LINES EXPRESSION (FREQUENCY f, SPATIAL ORDER m) IN ASYNCHRONOUS CASE (SYMMETRICAL TRIANGULAR CARRIER).

	m	f	f	f	f
F^{+}_{pwm}	$-2p$	$2f_c - 2f_s$	$4f_c - 2f_s$	$f_c + f_s$	$3f_c + f_s$
F^{-}_{pwm}	0	$2f_c$	$4f_c$	$f_c + 3f_s$	$3f_c + 3f_s$
F^{-}_{pwm}	0	$2f_c$	$4f_c$	$f_c - 3f_s$	$3f_c - 3f_s$
F^{+}_{pwm}	$2p$	$2f_c + 2f_s$	$4f_c + 2f_s$	$f_c - f_s$	$3f_c - f_s$

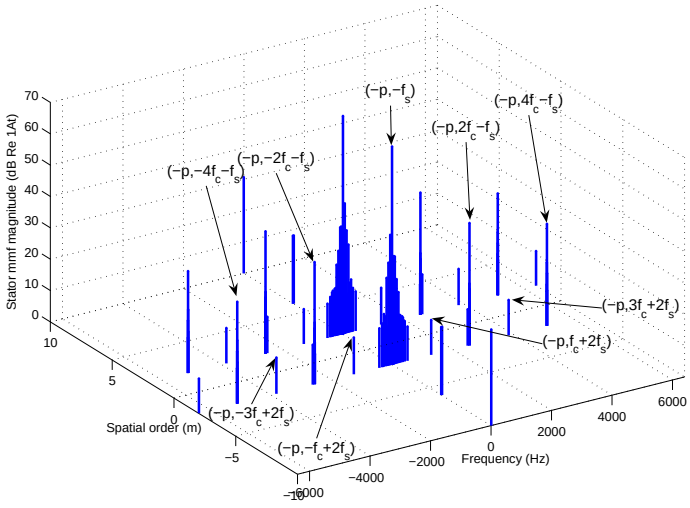

Fig. 2. Complex FFT of stator mmf $f^s_{mm}(t, \alpha_s)$ in asynchronous PWM case ($f_s = 50$ Hz, $f_c = 1280$ Hz, $p = 2$).

For instance, to find the PWM force lines associated to the current harmonics of frequencies $2f_c \pm f_s$, the stator mmf harmonics F_n to account for are a first mmf wave of spatial order $-p$ and frequency $-2f_c - f_s$ (which is equivalent to a spatial order p and frequency $2f_c + f_s$), and a second mmf wave of spatial order p and frequency $-2f_c + f_s$.

In the case of a symmetrical triangular carrier, the noisiest pure PWM lines are therefore centered around twice the switching frequency.

C. Experimental validation

1) PWM currents: A 250 kW squirrel-cage induction machine has been tested with an asynchronous PWM with $f_c = 1280$ Hz. The resulting PWM currents magnitudes are displayed in function of speed (which is proportional to the supply frequency, and therefore to the modulation index in the constant flux phase) in Fig. 3. Despite the current variations due to numerical errors during post-processing, the global evolution of PWM current magnitude agrees with results of Fig. 1 that comes from the analytical calculations of [13]. These experiments also confirm that the main PWM group at starting is the one around twice the switching frequency.

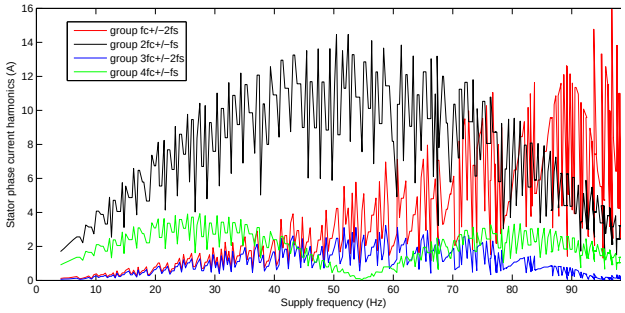

Fig. 3. Experimental stator current harmonic groups magnitude in functio.. of supply frequency (asynchronous regular sampling PWM, $f_c = 1280$ Hz).

2) Sound power level: In Fig. 4 is displayed the sound power level radiated by the motor at very low speed (150 rpm), so that magnetic vibrations linked to some slotting permeance harmonics (winding, slotting, saturation harmonics) have low frequencies and do not contribute to the global A-weighted sound power level. This fact can be observed in the experimental spectrum, as all the main acoustic lines are centered around multiples of the switching frequency, and are therefore generated by some current PWM harmonics.

The highest acoustic lines are centered around twice the switching frequency, where the PWM current harmonics magnitudes are the highest. In accordance with the magnitudes of PWM current harmonics, the other main acoustic lines appear near four times the switching frequency, once the switching frequency and three times the switching frequency.

On the bottom part of Fig. 4 is displayed an enlarged view of the sound power level spectrum around twice the switching frequency. The largest pure PWM lines (group number 1), which were previously determined analytically, correctly appear around $2f_c - 2f_s = 2550$ Hz (spatial order 2p), $2f_c = 2560$ Hz (spatial order 0) and $2f_c + 2f_s = 2570$ Hz (spatial order -2p). Other groups (4a,4b,5a and 5b) are some slotting PWM lines, which come from the combination of some slotting permeance space harmonics and some PWM current time harmonics [14], [12].

3) Pure PWM vibrations orders and frequencies: The expressions of main pure PWM vibrations spatial orders, frequencies and propagation directions have been validated by visualizing the stator deflections at some given frequencies (Operational Deflection Shapes, see Fig. 5) on the 250 kW motor with $p = 2$. These animations were obtained from the vibration data of several stator circumference points. The four lobes of $2p = 4$ spatial order rotating vibration waves can be clearly observed.

A similar behavior was observed at other frequencies (see for instance Fig. 6 for main PWM lines around four times the switching frequency).

III. Reduction of PWM noise

A. Low noise design rule

As seen in section II, a resonance can occur between the exciting magnetic forces and a stator circumferential mode at a frequency match condition, and a spatial order match condition.

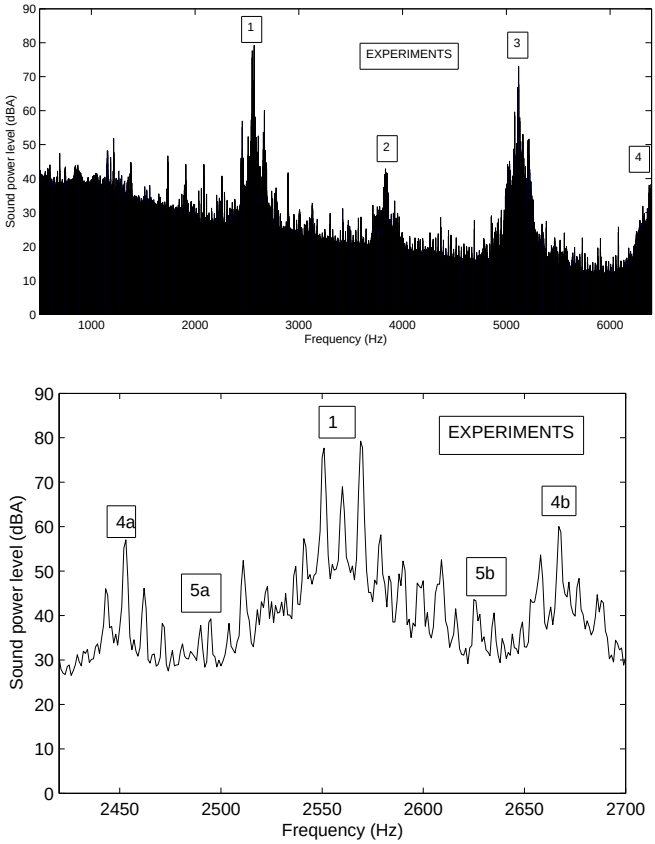

Fig. 4. Experimental A-weighted sound power level spectrum in asynchronous PWM case with f_s=5 Hz and f_c=1280 Hz (top: from 0 to 6400 Hz, bottom: from 2400 to 2700 Hz).

For regular sampling PWM, the switching frequency must be chosen so that $2f_c \pm 2f_s, 4f_c \pm 2f_s, ...$ groups do not meet the natural frequencies f_0 and f_{2p} of the stator stack on the whole motor speed range, i.e. for f_s lying from 0 to a certain maximal frequency f_{max}. This gives:

$$2f_c + 2f_{max} \ll f_{2p} \quad \text{or} \quad 2f_c - 2f_{max} \gg f_{2p} \tag{8}$$

and

$$2f_c \gg f_0 \quad \text{or} \quad 2f_c \ll f_0 \tag{9}$$

The meaning of $\ll$ can be quantified more precisely using an estimation of the modal damping coefficient ξ_m associated to mode m: assuming that the dynamic response of the stator structure is a second-order filter of critical frequency f_m and damping ξ_m, the gap between the exciting force frequency and the natural frequency should be more than the band-width $\xi_m f_m$. ξ_m can be determined using the experimental law of [8] ($\xi_m \approx 2\%$), which gives

$$2f_c + 2f_{max} \ll (1-\xi_{2p})f_{2p} \quad \text{or} \quad 2f_c - 2f_{max} \gg (1+\xi_{2p})f_{2p} \tag{10}$$

and

$$2f_c \ll (1-\xi_0)f_0 \quad \text{or} \quad 2f_c \gg (1+\xi_0)f_0 \tag{11}$$

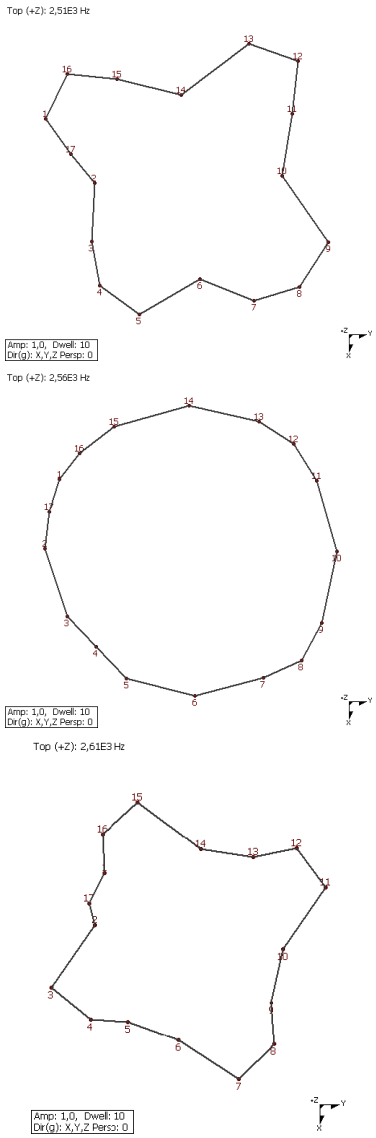

Fig. 5. Stator deflection shape at pure PWM vibration frequencies $2f_c - 2f_s = 2510$ Hz (top), $2f_c = 2560$ Hz (middle) and $2f_c + 2f_s = 2610$ Hz (bottom) for $f_c = 1280$ Hz and $f_s = 25$ Hz.

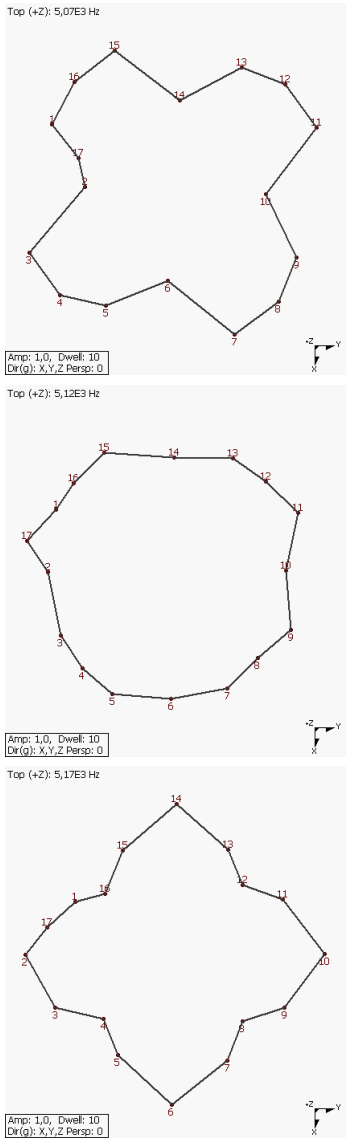

Fig. 6. Stator deflection shape at pure PWM vibration frequencies $4f_c - 2f_c = 5070$ Hz (top), $4f_c = 5120$ Hz (middle) and $4f_c + 2f_s = 5170$ Hz (bottom) for $f_c = 1280$ Hz and $f_s = 25$ Hz.

where the $\ll$ and $\gg$ mean a 100 Hz difference for a robust design.

These conditions are harder to fulfill in the synchronous phase, during which the switching frequency varies proportionally to the supply frequency. However, PWM noise is the noisiest at starting phase when f_s is close to 0, and where the strategy is necessarily asynchronous.

B. Natural frequencies computation

These rules can either be applied after the motor manufacturing, if the PWM strategy is not already fixed, or to change the PWM strategy in order to decrease noise. They can also be applied at motor design stage, and in that case one must estimate the motor natural frequencies in order to properly design the switching strategy.

A simple analytical model consists in modeling the stator structure as an equivalent ring whose width is given by the height of yoke, and whose mass density is the one of the stator stack corrected by the teeth and winding mass. The analytical expression of the breathing mode is then [15] given by

$$f_0 = \frac{1}{2\pi D_s}\sqrt{\frac{E_s}{K_f \Delta_m \rho_s}} \tag{12}$$

where D_s is the stator mean radius, K_f is the stator stacking factor, ρ_s the stator stack mass density and E_s is Young modulus, and Δ_m is the mass increase due to winding and teeth:

$$\Delta_m = 1 + \frac{W_{st} + W_{sw}}{W_f + W_{sy}} \tag{13}$$

where W_{st}, W_{sw}, W_f and W_{sy} respectively stand for the mass of stator teeth, winding, frame and yoke.

The natural frequency of the $2p$ mode can be obtained analytically with

TABLE III
CIRCUMFERENTIAL MODES NATURAL FREQUENCIES VALIDATION OF ANALYTICAL MODEL DIVA WITH 3D FEM.

Mode number n	DIVA	3D FEM
0	2870	2870
2	595	580
3	1535	1570
4	2885	2840

$$f_{2p} = K_{2p} f_0 \frac{h_s}{2\sqrt{3}D_s} \frac{2p(4p^2-1)}{\sqrt{4p^2+1}} \quad (14)$$

where h_s is the stator height of yoke, and K_{2p} is a corrective coefficient whose expression can be found in [15], [16], [17].

IV. APPLICATION

A. Theoretical quietest switching frequency

The analytical model applied to the 250 kW traction motor gives $f_0 = 2890$ Hz and $f_{2p} = 2850$ Hz. These two frequencies are quite close, which is not surprising as $K_{2p} \approx 1$, so that for $p = 2$ one obtains

$$\frac{f_{2p}}{f_0} \approx 4.2 \frac{h_s}{D_s} \quad (15)$$

Therefore, if $h_s \approx D_s/4$, mode 0 and 4 occur at similar natural frequencies. The fact that these two frequencies are close one from each other makes it more important to avoid resonances with PWM forces.

A modal experimental analysis was run in order to validate the calculation of these two frequencies, but the motor deflection shapes at these high frequencies were too complex to be easily associated to a pure circumferential ring mode. Natural frequencies were therefore validated by comparison with a solid FEM model of the stator stack equivalent cylinder (Table III).

Applying rules of (10) and (11), the switching frequency must be chosen so that

$$2f_c + 2f_{max} \ll f_{2p} - \xi_{0,2p} f_{0,2p} \Rightarrow f_c \ll 1290\text{Hz} \quad (16)$$

or

$$2f_c - 2f_{max} \gg f_{0,2p} + \xi_{0,2p} f_{0,2p} \Rightarrow f_c \gg 1610\text{Hz} \quad (17)$$

Therefore, the value of 1280 Hz should not be the optimal value in order to limit PWM noise: it should decrease either with a lower switching frequency near 1100 Hz, or with a much higher switching frequency near 1900 Hz. The value $f_c = f_0/2 = 1495$ Hz is the worst choice, as the corresponding 0 order exciting forces frequencies do not change with speed.

B. Experimental validation

To validate these conclusions, some experiments have been run on another 250 kW traction motor whose rotor has been designed in order to cancel main saturation and slotting harmonics [3], [2]: no magnetic resonance occurred when feeding the motor with sinusoidal currents. The motor has been run at variable-speed with asynchronous PWM, by linearly increasing its supply frequency from 0 to $f_{max} = 105$ Hz. Some run-ups were measured with different switching frequencies varying from 600 to 1900 Hz, the default switching frequency being 1280 Hz. Results are displayed in Fig. 7.

On the upper part of this figure, the sound pressure level is displayed as a function of time (proportional to speed) for the different switching frequencies. From 0 to 30 km/h, the acoustic level strongly changes, and some resonances occur: the global noise level is dominated by pure PWM noise. Over 30 km/h, all the acoustic levels are the same, which shows that the measurements are independent of the switching frequency: the global noise level is dominated by non-magnetic noise sources, and especially fan noise. One of the quietest motors are the ones with $f_c = 1900$ Hz or 1800 Hz, whereas the noisiest motors are with $f_c = 1500$ Hz or 1600 Hz. A 15 dB difference can be observed during starting between the quietest and the noisiest PWM strategies, which shows that the choice of the switching frequency has a strong influence on acoustic noise.

On the lower part of Fig. 7 are displayed the average sound power level and the maximum sound power level observed from 0 to 30 kph in function of the asynchronous switching frequency. This graph clearly shows the resonance effect due to the frequency match between 0 or 4 order exciting PWM forces with the stator mode 0 or 4 natural frequency. The worse case is observed for a 1500-1600 Hz switching frequency, in good agreement with the analytical prediction of 1495 Hz.

V. CONCLUSION

The main source of magnetic noise due to PWM supply in induction machines has been analytically characterized, and validated by experiments. A low noise design rule, based on an analytical model of the stator natural frequencies, has been proposed and applied to a 250 kW traction motor. Experimental results show that the PWM resonances were correctly predicted, and that the proposed switching frequencies decreased noise radiation. Furthermore, a 15 dB variation was measured between the quietest and the noisiest switching frequencies: this great influence of the switching frequency can be explained by the fact that the 0 and $2p$ natural frequencies are close one from each other on the studied traction motor. The new asynchronous switching frequency of 1000 Hz reduces the noise level of 5 dB during starting, compared to the 1280 Hz default value, and reduces inverter switching losses at the same time.

Future work will investigate the psycho-acoustic impact of various PWM spread-spectrum strategies [18], [19], [20].

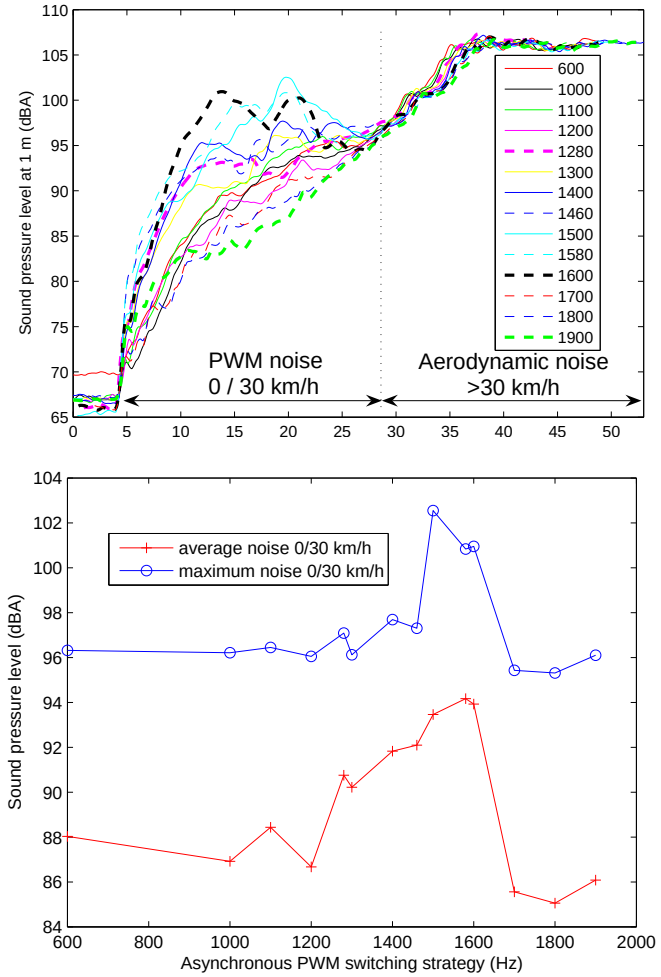

Fig. 7. Sound pressure level of prototype during starting phase, using various switching frequencies (up: noise level in function of time, bottom: maximum and average noise levels from 10 to 50 Hz). The default asynchronous PWM switching frequency used on the industrial traction motor is 1280 Hz.

REFERENCES

[1] J. Le Besnerais, V. Lanfranchi, M. Hecquet, and P. Brochet, "Optimal slot numbers for magnetic noise reduction in variable-speed induction motors," 2009, submitted to IEEE Trans. on Mag.

[2] J. Le Besnerais, V. Lanfranchi, M. Hecquet, R. Romary, and P. Brochet, "Optimal slot opening width for magnetic noise reduction in induction motors," *IEEE Trans. on En. Conv.*, accepted for publication.

[3] J. Le Besnerais, V. Lanfranchi, M. Hecquet, G. Lemaire, E. Augis, and P. Brochet, "Charaterization and reduction of magnetic noise due to saturation in induction machines," *IEEE Trans. on Mag.*, accepted for publication.

[4] W. Lo, C. Chan, Z. Zhu, L. Xu, D. Howe, and K. Chau, "Acoustic noise radiated by PWM-controlled induction machine drives," *IEEE Trans. on Industrial Electronics*, vol. 47, no. 4, pp. 880–889, Aug. 2000.

[5] P. Alger, *Induction machines : their behaviour and uses*. Gordon and Breach Science Publishers, 1970.

[6] P. Timar, *Noise and vibration of electrical machines*. Elsever, 1989.

[7] H. Jordan, *Electric motor silencer - formation and elimination of the noises in the electric motors*. W. Giradet-Essen editor, 1950.

[8] S. J. Yang, *Low noise electrical motors*. Oxford: Clarendon Press, 1981.

[9] W. Soedel, *Vibrations of shells and plates*. Marcel Dekker, 1993.

[10] S. Verma and A. Balan, "Determination of radial-forces in relation to noise and vibration problems of squirrel-cage induction motors," *IEEE Trans. on En. Conv.*, vol. 9, no. 2, pp. 404–412, June 1994.

[11] G. Bossio, C. D. Angelo, J. Solsona, G. Garcia, and M. Valla, "A 2-D model of the induction machine: an extension of the modified winding function approach," *IEEE Trans. on Energy Conversion*, vol. 19, no. 1, pp. 62–67, Mar. 2004.

[12] J. Le Besnerais, V. Lanfranchi, M. Hecquet, P. Brochet, and G. Friedrich, "Characterisation of the radial vibration force and vibration behaviour of a PWM-fed fractional-slot induction machine," *IET Electric Power Applications*, Feb. 2009.

[13] S. Ueda, K. Honda, T. Ikimi, M. Hombu, and A. Ueda, "Magnetic noise reduction technique for an AC motor driven by a PWM inverter," *IEEE Trans. on Power Electronics*, vol. 6, July 1991.

[14] J. Le Besnerais, "Reduction of magnetic noise in PWM-supplied induction machines – low-noise design rules and multi-objective optimisation," Ph.D. dissertation, Ecole Centrale de Lille, France, Nov. 2008.

[15] J. Gieras, C. Wang, and J. Lai, *Noise of polyphase electric motors*. CRC Press, Dec. 2005.

[16] M. Anwar and I. Hussain, "Radial force calculation and acoustic noise prediction in switched reluctance machines," *IEEE Trans. on Ind. App.*, vol. 36, no. 6, pp. 1589–1597, 2000.

[17] K. Maliti, "Modelling and analysis of magnetic noise in squirrel-cage induction motors," Ph.D. dissertation, Stockholm, 2000.

[18] K. Borisov and A. M. Trzynadlowski, "Experimental investigation of a naval propulsion drive model with pwm-based attenuation of the acoustic and electromagnetic noise," *IEEE Trans. on Ind. Elec.*, vol. 53, no. 2, 2006.

[19] J.-Y. Chai, Y.-H. Ho, Y.-C. Chang, and C.-M. Liaw, "On acoustic-noise-reduction control using random switching technique for switch-mode rectifiers in pmsm drive," *IEEE Trans. on Industrial Electronics*, vol. 55, no. 3, pp. 1295 – 1309, Mar. 2008.

[20] V. Lanfranchi, G. Friedrich, J. Le Besnerais, and M. Hecquet, "Spread spectrum strategies study for induction motor vibratory and acoustic behavior," in *Proceedings of the IECON*, Nov. 2006.

Jean Le Besnerais received its Master in Engineering, Applied Mathematics, in 2005 at the Ecole Centrale Paris, France. He then obtained his Ph.D. degree in Electrical Engineering in 2008 at the Laboratoire d'Electrotechnique et d'Electronique de Puissance (L2EP, http://l2ep.univ-lille1.fr/), Ecole Centrale de Lille, in the Optimization team. His research interests include analytical modeling of induction machines, magnetic noise and vibration issues in PWM-fed electrical machines, and optimization methods.

Vincent Lanfranchi received his Ph.D. degree in electrical engineering from the University of Reims (France) in 2000. Since 2001 he has been an Associate Professor at the Universite de Technologie de Compiegne. His teaching areas are electrical engineering and mechatronics. He is a researcher in the LEC laboratory (Laboratoire d'Electromécanique de Compiègne). His main research interests are converter-machine interactions and Pulse Width Modulation strategies.

Michel Hecquet received his Ph.D. degree in electrical engineering from the University of Lille, France, in 1995. His research interests include the modeling, the design and the optimization of electrical machines, particularly the application of the experimental designs methodology to finite element models. He is interested in the development and application of multi-physics models of electrical machines (electromagnetic, mechanical and acoustic) in view of their optimal design. He is now working in the L2EP as an associate professor and researcher.

Pascal Brochet received a Ph.D. in Numerical Analysis in 1983 at the Université des Sciences et Technologies de Lille. He worked during seven years in an Automotive Equipment Company as a research engineer in the field of computer aided design of electrical machines. He then joined the Ecole Centrale de Lille in 1990 where he is now full professor and researcher at the L2EP laboratory. His main interests are numerical simulation, design and optimization of electrical machines.